Laser à Mode de Galerie en Verres Fluorés Dopés Erbium

Patrice Feron

Whispering Gallery Mode Lasers in Erbium doped fluoride glasses

Patrice Féron

GIS "FOTON" Laboratoire d'Optronique (CNRS-UMR 6082)
ENSSAT 6 rue de Kerampont, 22300 Lannion, France

ABSTRACT. Light can be confined efficiently in the high quality factor (Q), small volume whispering-gallery-modes observed in spherical dielectric microresonators. The properties of these modes allow to obtain laser action in Rare-Earth doped glass spheres. After a brief introduction to the physics of the whispering-gallery modes, we describe recent experiments on the lasing properties of doped microspheres at room temperature.

P.A.C.S.: 42.55.Sa; 42.55.Xi; 42.60.Da

1 Introduction

Since a few years optical microspherical cavities are subject to numerous studies[1]. In dielectric spheres light can be guided through whispering-gallery-modes (WGMs). The unique combination of strong temporal and spatial confinement of light makes these systems of interest for a number of fundamental research[2] and an attractive new building block for fiber optics and photonics applications. Many experiments have been performed on microdroplets showing various cavity-enhanced and/or nonlinear optical effects including laser action[1]. However, experiments with droplets suffer from their short lifetime which is a severe restriction for applications. Since the first laser oscillation in a solid state sphere demonstrated by T. Baer with large Nd:YAG spheres (diameter $5mm$)[3], laser action has been obtained in many different rare-earth doped glass spheres [4, 5, 6]. Our experiments are focused on the optical transition ${}^4I_{13/2} \longrightarrow {}^4 I_{15/2}$ around $1.55\mu m$ of Erbium doped fluoride glass, which offers potential applications in telecommunications. In this review, after

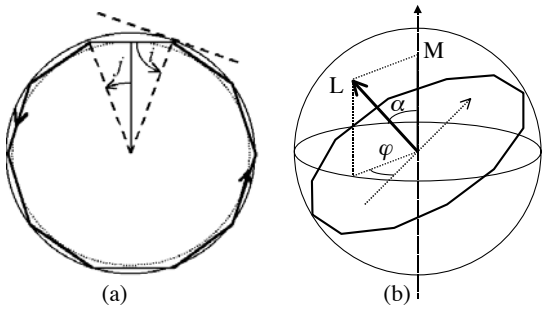

Figure 1: (a)Ray of light propagation by TIR. Definition of complementary angles i and j. (b) Angular momentum associated to a WGM and its M projection on polar axis

a brief introduction to WGMs we describe experimental results on laser oscillations obtained with different coupling schemes.

2 General properties of Whispering-Gallery Modes

2.1 Geometric Optics and Eikonal equation

In the optical domain, whispering-gallery modes can be viewed as high angular momentum electromagnetic modes in which light propagates by repeated total internal reflection (TIR) surface at grazing incidence with the proper phase condition after circling along the sphere surface. Consider a microsphere of radius a with refractive index N and a ray of light propagating inside, hitting the surface with angle of incidence i (Fig.1(a)). If $i > i_c = \arcsin(1/N)$, then total internal reflection occurs. Because of spherical symmetry, all subsequent angles of incidence are the same, and the ray is trapped. This simple geometric picture leads to the concept of resonances. For large microspheres ($a >> \lambda$), the trapped ray propagates close to the surface, and traverses a distance $\approx 2\pi a$ in a round trip. If one round trip exactly equals ℓ wavelengths in the medium (ℓ = integer), then one expects a standing wave to occur. This condition translates into $2\pi a \approx \ell\,(\lambda/N)$ since λ/N is the wavelength in the medium. In terms of size parameter the resonance condition is $x = 2\pi a/\lambda \approx \ell/N$. The number of wavelengths ℓ in the circumference can be identified as the angular momentum in the usual sense. Indeed, let us consider the ray in figure.1(a) as a photon. Its momentum is $p = \hbar k =$

$\hbar 2\pi N/\lambda$ where k is the wave number. If this ray strikes the surface at near-glancing incidence ($i \approx \pi/2$), then the angular momentum, denoted as $\hbar\ell$, is $\hbar\ell \approx ap = a2\pi\hbar N/\lambda$. For lower incidences, one expects other resonances at frequencies very close and characterized by the radius of the caustic $r_1 = a\ \cos j$ under condition ($a/N < r_1 < a$).

A first step to a wave description consists to study the properties of the phase $S = \int_{r_o}^{r} k_o N(r) ds$ of a scalar field $\Phi \approx \exp(iS)$ using the Eikonal equation $(\vec{\nabla} S)^2 = N^2(r) k_0^2$. Considering the momentum $\vec{p} = \vec{\nabla} S$ the spherical symmetry leads to the conservation of the angular momentum $\vec{L} = \vec{r} \times \vec{\nabla} S$. The azimuthal angle φ being a cyclic variable for this problem $L_z = \partial S/\partial\varphi$ ($\vec{L}$ projection on z axis) and $\left|\vec{L}\right| = L = r_1 k_o N$ are constants. We can separate S as $S_1(r).S_2(\theta).S_3(\varphi)$ and the angular motions correspond to a uniform precession of φ and an oscillation for θ between the two values $\theta = \pi/2 \pm \alpha$ with $\alpha = \arccos(|M|/L)$ (Fig.1(b)). Taking into account the Goos-Hänchen effect, we can consider a TIR on an effective radius $a_{eff} = a + \delta_P$ with δ_P polarization dependent. Thus we can see the radial motion as an oscillation between $r_1 \equiv L/k_o N$ (radius of the internal caustic[1]) and $r = a_{eff}$. On each caustic, the reflected wave reaches [7] a phase $\Delta\Phi_c = -\pi/2$ ($2\times$ for θ, $1\times$ in r_1). Over one period, each S_i reaches ΔS_i given by $\Delta S_3 = 2\pi\,|M|\,, \Delta S_2 = 2\pi\,(L - |M|) - \pi, \Delta S_1 = 2\pi\ f\,(N k_o a_{eff}/L) - 3\pi/2$ with $f(u) = \sqrt{u^2 - 1} - \arccos(1/u)$.

WGM corresponds to a phase-matching after a round trip and leads to have each partial phase ΔS_i equals to $2\pi \times integer$. First, we obtain the classical quantization for the angular momentum with ℓ and m, respectively angular and azimuthal quantum numbers: $M = m$ with $-\ell \leq m \leq \ell$ and $L \approx \ell + 1/2 (\ell >> 1)$. The phase-matching condition on radial direction leads to introduce a radial number n such as

$$\frac{L}{\pi} f\left(\frac{N k_o a_{eff}}{L}\right) = n - \frac{1}{4} \tag{1}$$

The radial number $n = 1, 2, 3, \cdots$corresponds to number of oscillations between r_1 and a_{eff}. At a given polarization n, ℓ, m characterize the resonances. For a perfect sphere there is not particular quantization axis, this leads to m independence. The ellipticity e of the sphere leads

[1] Moreover the radial equation leads to an external caustic with radius $r_2 \equiv L/k_o \approx Na$ in the external medium ($N = 1$)

to a non degeneracy of m values and the positions of resonances, in term of size parameter and $\nu = \ell + \frac{1}{2}$, can be resumed as [8] :

$$\begin{aligned} Nx^P_{n,l,m} \approx & \left[\nu + \left(\frac{\nu}{2}\right)^{\frac{1}{3}} \left[\frac{3\pi}{2}\left(n - \frac{1}{4}\right)\right]^{\frac{2}{3}} - \frac{P}{\sqrt{N^2-1}}\right] \\ & \times \left[1 + \frac{e}{3}\left(1 - 3\frac{\ell - |m|}{\ell}\right)\right] \end{aligned} \tag{2}$$

with $P = N$ for TE modes and $P = N^{-1}$ for TM modes. This equation allows to precise the main characteristics of WGM spectrum. First, the spectrum is quasi-periodic *versus* ℓ, this corresponds to a pseudo-Free Spectral Range (FSR) $\Delta_0 = c/2\pi Na$. Second, the spacing between modes having same quantum numbers but different polarizations is $x^{TM}_{n,\ell} - x^{TE}_{n,\ell} = \sqrt{N^2-1}/N^2$. The greatest change of frequency is produced by variation of n (as example with $\ell \approx 250$ the mode separation $\sim 10\Delta_0$) it decreases when n values grow up. Small ellipticities lead to a quasi-equidistant mode family characterized by $\Delta\nu/\Delta\,|m| = e\ \Delta_0$.

2.2 The electromagnetic problem

Following the Hansen's method [9] solutions of the vectorial Helmholtz equation have angular dependence described by vectorial spherical harmonics defined as :

$$\begin{cases} \vec{Y}^{(m)}_{\ell m} = \vec{\nabla} Y^m_\ell \times \vec{r} \Big/ \sqrt{\ell(\ell+1)} & : \text{ noted } \ \vec{X}^m_\ell \\ \vec{Y}^{(e)}_{\ell m} = r\vec{\nabla} Y^m_\ell \Big/ \sqrt{\ell(\ell+1)} & : \text{ noted } \ \vec{Y}^m_\ell \\ \vec{Y}^{(o)}_{\ell m} = Y^m_\ell \hat{r} & : \text{ noted } \ \vec{Z}^m_\ell \end{cases} \tag{3}$$

superscripts (m) and (e) correspond to the magnetical or electrical character of the radiated field by the ℓ order multipole. They are respectively associated to TE and TM modes. Superscript (o) corresponds to the radial character of the corresponding field. Formally we can express the fields for both polarizations :

$$\begin{cases} \vec{E}^{TE}_{\ell m}(\vec{r}) = E_o \frac{f_\ell(r)}{k_o r} \vec{X}^m_\ell(\theta,\varphi) \\ \vec{B}^{TE}_{\ell m}(\vec{r}) = -\frac{iE_o}{c}\left(\frac{f_\ell(r)}{k_o^2 r}\vec{Y}^m_\ell(\theta,\varphi) + \sqrt{\ell(\ell+1)}\frac{f_\ell(r)}{k_o^2 r^2}\vec{Z}^m_\ell(\theta,\varphi)\right) \end{cases} \tag{4}$$

$$\begin{cases} \vec{E}^{TM}_{\ell m}(\vec{r}) = \frac{E_o}{N^2}\left(\frac{f_\ell(r)}{k_o^2 r}\vec{Y}^m_\ell(\theta,\varphi) + \sqrt{\ell(\ell+1)}\frac{f_\ell(r)}{k_o^2 r^2}\vec{Z}^m_\ell(\theta,\varphi)\right) \\ \vec{B}^{TM}_{\ell m}(\vec{r}) = -\frac{iE_o}{c}\frac{f_\ell(r)}{k_o r}\vec{X}^m_\ell(\theta,\varphi) \end{cases} \tag{5}$$

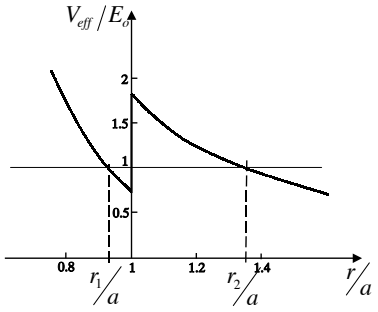

Figure 2: Effective potential for an equivalent particle and turning point for fundamental energy E_o, $(n = 1, x = 74.4)$

With $f_\ell(r) = \psi_\ell(Nk_or)$ for $r < a$ and $f_\ell(r) = \alpha\psi_\ell(k_or) + \beta\chi_\ell(k_or)$ for $r > a$. $\psi_\ell(\rho) = \rho\ j_\ell(\rho)$ and $\chi_\ell(\rho) = \rho\ n_\ell(\rho)$ where j_ℓ and n_ℓ are respectively spherical Bessel and Neumann functions. In fact the radial equation is very similar to the Schrödinger equation with a pocket-like pseudo-potential due to the refraction index discontinuity $N - 1$ at the surface of the sphere (Fig.2). This effective potential approach thoroughly analyzed by Nussenzveig [10] provides good physical insight in many properties of the WGM's which appear as quasi-bound states of light, analogous to the circular Rydberg states of alkali atoms. the radial number n gives the number of peaks in the radial distribution of the field inside the sphere. It corresponds to the radial index in the Eikonal approach. The lowest-lying state is confined near the bottom of the potential well, *i.e.* as close as possible to the surface of the sphere, and is expected to occur for $\ell \approx Nka \approx Nx$, the maximum value of the angular momentum. Light trapped into these mode can escape out of the sphere only by tunneling across the potential barrier which extends as far as Na for this state. The very long evanescent tail of this quasi-bound state implies a very weak coupling to the outside $N = 1$ medium and extremely high Q factors. The quasi-bound state energy domain is limited, thus, only few n values correspond to WGM.

2.3 Approximated positions of resonances

Continuity of tangential components of the fields allows to find equations for the positions of resonances. By going through the standard Mie

scattering formalism [11] and imposing the condition that the phase shift δ satisfies $\exp(2i\delta) = -1$ ($\equiv \alpha = 0$), the resonance condition can be written as :

$$P\frac{J_\nu^{'}(Nx)}{J_\nu(Nx)} = \frac{N_\nu^{'}(x)}{N_\nu(x)} \tag{6}$$

where $P = N$ for TE polarization ($P = N^{-1}$ for TM) and $\nu = \ell + 1/2$ comes about in translating the spherical Bessel and Neumann functions to their cylindrical counterparts. The quantities in eq.6 can be expressed as asymptotic series in powers of $\nu^{-1/3}$[12]. This leads to the first terms of the resonances expressed in size parameter :

$$Nx_{n,\ell} = \ell + 1/2 - \left(\frac{\ell + 1/2}{2}\right)^{1/3} \alpha_n - \frac{P}{\sqrt{N^2 - 1}} + ... \tag{7}$$

where α_n are zeros of Airy function $A_i(-z)$.

3 Experiments

3.1 Fabrication of microspheres

We have developed a process using a microwave plasma torch which allows to produce silicate or fluoride glass spheres from powders.The plasma is generated using a microwave supply with a nominal oscillator frequency of $2.4GHz$ and a maximum power of $2kW$. Argon is used as plasma gas and oxygen or nitrogen as sheath gas. Powders are axially injected and melt when passing through the plasma flame, superficial tension forces giving them their spherical form. Free spheres are collected a few ten centimeters lower. The diameter of the spheres depends essentially on the powder size and varies from 10 to $200\mu m$. We can adjust the microwave power and gas discharges to obtain optimal conditions to spheroidize fluoride or silicate glass. We obtain free spheres using our fusion technique. Then, they are glued at the tip of optical fibers ($20\mu m$ in diameter) which allow to manipulate them easily and to insert them in the optical setup.

3.2 Excitation of WGMs

For passive microspheres many coupling techniques, such as prisms[13], tapered fibers[14],half block couplers, angle polished fiber couplers and

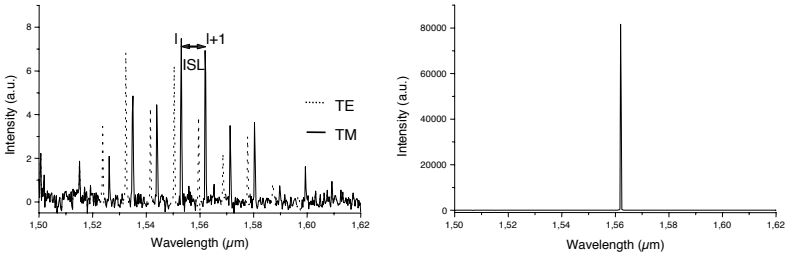

Figure 3: (a)Fluorescence spectrum (b) laser effect at 1562 nm

waveguides [15] have been experimentally demonstrated. Efficient coupling to WGMs not only requires to adjust the frequency of the excitation beam to a WGM resonance. The excitation beam should also have an angular momentum (with respect to the center of the sphere) which matches the angular momentum of this mode.If we are interested to the most confined modes with low radial numbers, only frustrated total internal reflection provides an efficient excitation scheme. It can be achieved with a high-index prism (with index N_p) nearly in contact with the sphere if the incident beam hits the prism surface with an angle θ close to the critical angle $\arcsin(N/N_p)$ so that its angular momentum is $N_p ka \sin\theta \approx Nka$. Spheres can be set very close to the prism in the evanescent wave domain, the distance being controlled with micropositioning and with piezoelectric actuators. Our experiments are focused on the optical transition ${}^4I_{13/2} \longrightarrow {}^4 I_{15/2}$ at $1.55\mu m$ of Erbium doped spheres. Among the different pumping wavelengths which can be used ($810nm$, $975nm$ and $1.48\mu m$)[16], we chose $1.48\mu m$ in order to obtain a good overlap between the pump and laser mode volumes. The pump laser is a multimode laser diode operating around $1.48\mu m$ focused onto the surface of a SF11 prism with a high-index of refraction. When pumping with an angle that provides a TIR we couple light in the sphere by an optical tunneling effect. The non absorbed pump beam and the fluorescence (or laser) signal corresponding to the WGMs of the sphere are separated with a demultiplexing device ($1480nm/1550nm$). Thus we can analyze simultaneously the pump and the fluorescence (or laser) signals. Figure 3 presents results obtained with a microsphere $56\mu m$ in diameter

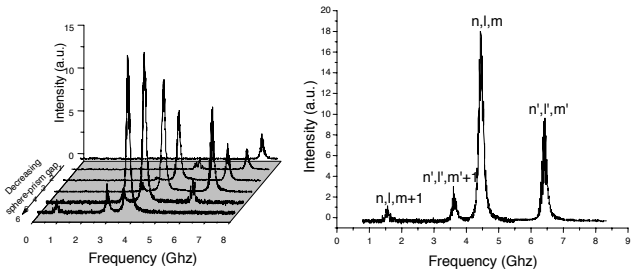

(a) (b)

Figure 4: (a) Spectra for different gap values (b) laser action for two families of peaks differing by n, ℓ and m values

doped with 0.2% by weight of Erbium. The spectral characteristics of the emission around $1.55\mu m$ were analyzed with a $0.1nm$ resolution optical spectrum analyzer (OSA) directly connected after demultiplexing. The fluorescence spectrum around $1.55\mu m$ (Fig.3.a) presents a discrete feature, which is characteristic of the collection through WGMs, with mainly two series of peaks associated to TE and TM modes. According to Eq.7 the FSR can be approximated by $\Delta\nu = c/2\pi N_s a = 1137\ GHz$ (measured as $1120 \pm 20GHz$) and the spacing between TE and TM is $810 \pm 20GHz$ close to the calculated $\Delta\nu_{TE,TM}$. By increasing the pump intensity while keeping the sphere-prism gap close to zero, we observed laser oscillations for only one TM polarized peak on the OSA spectrum (Fig.3.b). By varying the sphere-prism gap with a piezo-actuator, we obtained multimode laser oscillations. Laser modes can be selected and optimized by adjusting the gap. When the sphere is close to the prism, only TM modes of low wavelengths oscillate because of the higher losses for TE and higher wavelength modes. For larger gaps, TE and TM modes oscillate simultaneously. With sphere close to the prism (few tens of nanometers), close examination of the TM peak at $1.562\mu m$ was possible using a Fabry Perot ($FSR = 10\ GHz$, finesse= 170). Figure 4.a shows that lasing modes change when varying the sphere-prism gap. When superposing two of these spectra (Fig.4.b), we obtain 4 peaks distinguished by (n, ℓ) and (n', ℓ'). A more detailed examination of these modes was carried out using a fibre Fabry Perot interferometer (FSR of $10MHz$, finesse= 70). The pump intensity was fixed at more than

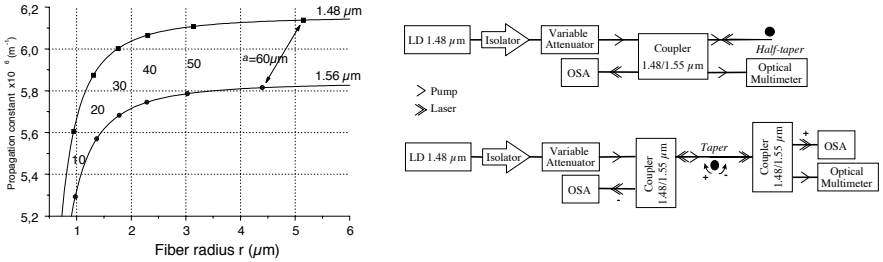

Figure 5: (a) propagation constants β_f (curves) and β_s (dot) of WGMs ($n = 1$) for different radii. (b) Experimental setups for coupling by taper or half taper

five times the threshold level ($< 600\mu W$) and the gap was adjusted to maximize the laser output intensity for better detection. The linewidths were measured to be around $270KHz$.

3.3 Coupling by tapered fiber

The laser effect can also be obtained, using tapers[17] or half-tapers for direct fiber coupling[18]. Coupling of ZBLAN microspherical lasers differs on two main points from coupling of passive silica spheres: (i) the refractive index of the sphere materials are different, $N_s \cong 1.5$ ($\cong 1.45$) for ZBLAN (silica) at wavelength $\lambda = 1.55\mu m$ (ii) the optimum coupling with two wavelengths, $\lambda = 1.48\mu m$ for the pump and $\lambda = 1.56\mu m$ for the laser signal is not the same. Using the method described by Knight[14] we calculated how to match the propagation constant of the appropriate mode in the tapered fiber to the propagation constant of the WG modes at the surface of the sphere for both wavelengths. These calculations were made for a fiber drawn gradually to form a narrow thread but they also can be used for a fiber tapered till the break (half-taper). Calculations show that a good coupling is obtained for those spheres characterized by specific (N_s, a) for wavelengths λ. Results (fig.5.a) for the propagation constant β_s of the WG modes $n = 1$ are plotted for different sphere radii and show that in our case, as the pump wavelength is close to that of the laser field, a single taper or half-taper allows to couple both fields in and out the microspherical laser. The experimental setup

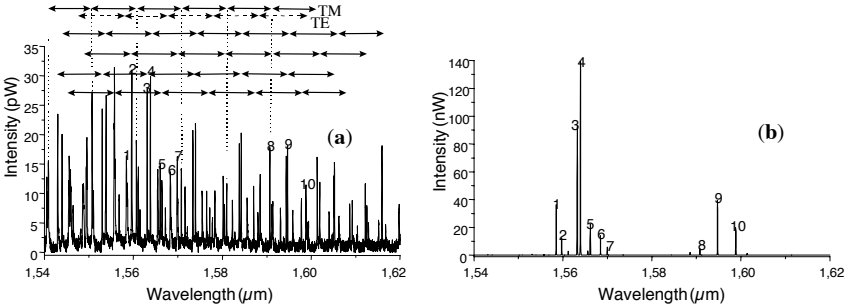

Figure 6: Sphere of $53\mu m$ in diameter (a) Fluorescence (b) laser spectra.

(fig.5.b) was realized with standard fiber-optic components spliced or connected with APC connectors. Spheres were mounted on x-y-z stages microcontroled to bring the equator region in contact with the evanescent field surrounding the taper. For any sphere diameters we observed an enhancement of the fluorescence intensity and a higher peak density than those obtained with a prism. It is obvious that the propagation in the taper, its non constant diameter and consequently variable gap between the fiber and the microsphere, lead an half-taper coupling to be less selective than a prism coupling. However for diameter $53 \pm 1\mu m$, we made an analysis similar to that used for excitation by prism for the fluorescence spectrum around $1.56\mu m$ (Fig.6.a). This standard analysis shows that these series of peaks (75 peaks with $0.1nm$ resolution) can be assigned to seven families of modes, each of them having the same radial order and different polarizations. We have reported only few $\Delta\nu$ for the five families (differing by n) which led to laser oscillations. When increasing the pump intensity we obtained multi-mode laser oscillations (fig.6.b).

3.4 Application: Linewidth narrowing of a semi-conductor laser

When a (slave) laser is injected by an external laser field which is a coherent source (master laser), it can find a phase reference which is more or less strong following the relative amplitudes of both sources. Its linewidth can thus be strongly modified by the injection field [19], whose spectral density is essentially lorentzian and fixed by the master laser. Under frequency-locking conditions, the slave laser has the same

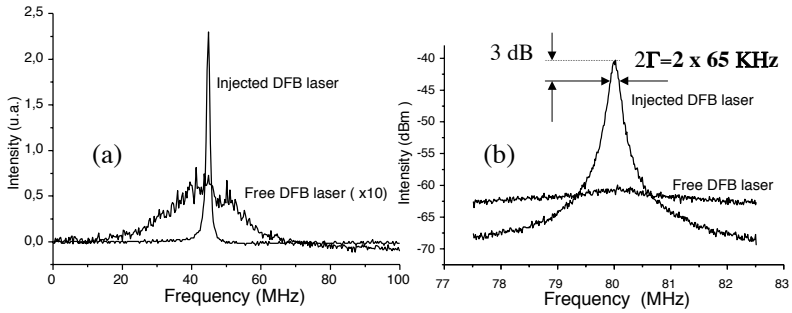

Figure 7: (a) Output FP spectra of the DFB laser. (b) Linewidths for free running and injected DFB laser after delayed self heterodyne detection

linewidth as the master. The laser signal from a microsphere ($95\mu m$ in diameter) with linewidth of the order of $50 - 100\ KHz$ is injected in a DFB laser. An isolator is used to avoid feedback in the microsphere laser. The signal which corresponds to the response of the injection, is collected from the other DFB facet and is analyzed with a Fabry-Perot (FP) interferometer ($FSR = 300\ MHz$, resolution $3MHz$). A finer spectral analysis can be achieved with a delayed self heterodyne detection of the optical signal followed by a spectral analysis of the beating electrical signal [20]. When the injected power is high enough ($10nW$ in our case) and the detuning equal to zero, we observed a frequency locking and a spectral purity transfer from the WGM to the DFB laser. This value of injected power represents the total optical power of the microspherical laser available at the output of the lensed-fiber. Figure 7.a presents the Fabry-Perot spectrum of the free running DFB, superposed to the spectrum when it is injected. The free DFB has a linewidth of $30MHz$ and the linewidth of the injected DFB laser is 65 KHz(Fig.7.b).

4 Red-shift due to pump intensity in Er:ZBLALiP WGM lasers

Realization of WGM laser needs glass in small amounts. We have made experiments on different glass samples with a new kind of Erbium doped heavy fluoride glass (Er:ZBLALiP) and doping rate varying from 0.01 $mol.\%$ to 6 $mol.\%$. For every doping rate we tested a few tens of spheres. Laser oscillations around 1550 nm were obtained for

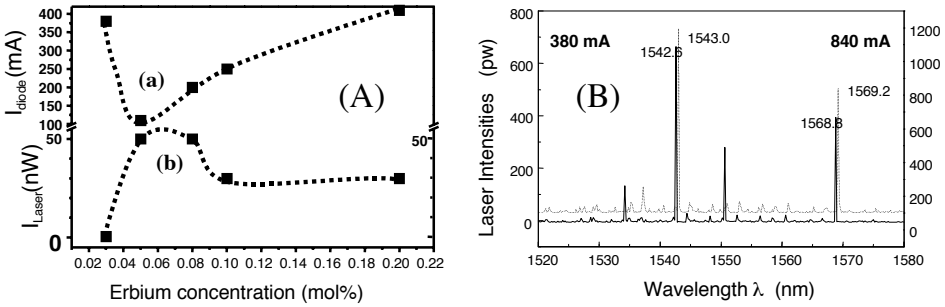

Figure 8: A-(a)Driving current for the pump at threshold.(b) main WGM laser line intensity. B-Red-Shift of WGM laser spectra of Er:ZBLALiP sphere (0.05 $mol.\%$)$2a = 60\mu m$

different Erbium concentrations (from 0.03 $mol.\%$ to 0.2 $mol.\%$) with an optimal concentration between 0.05 and 0.08 $mol.\%$. Such concentrations lead to an extended laser domain, lower thresholds and a better efficiency than other concentrations (Fig.8.A). Red-shift effect on the frequencies of both fluorescence and laser spectra (Fig.8.B) is experimentally observed when the pump power is increased, originating from thermal effects. A spectroscopic technique based on the green upconversion fluorescence[21] is used to compute a loading effective temperature for the Er:ZBLALiP microsphere and this further allows us to calibrate the properties of the microsphere laser in terms of the thermal expansion as well as the variation of the refractive index.

5 Acknowledgements

The author thanks F. Lissillour, G. Stéphan, R. Gabet , P. Besnard, Z.P. Cai, H.Y. Xu, M. Boustimi and M. Mortier for their contributions to these works.

References

[1] R.K. Chang, A.J. Campillo, *Optical processes in microcavities*, Singapore, World Scientific, 1996.

[2] L. Collot, V. Lefèvre-Seguin, M. Brune, J.M. Raimond, S. Haroche, Europhys. Lett. **23** p.327 (1993).

[3] T. Baer, Opt. Lett. **12** p. 392 (1987).
[4] V. Sandoghdar, F. Treussart, J. Hare, V. Lefèvre-Seguin, J.M. Raimond, S. Haroche, Phys. Rev. **A-54** p.1777 (1996).
[5] (a) K. Miura, K. Tanaka, K. Hirao, J. Non-Crys. Solids **213-214** p. 276 (1997). (b) M. Cai, K. Vahala, Opt. Lett. **25** p.260 (2000).
[6] (a) F. Lissillour, P. Féron, N. Dubreuil, P. Dupriez, G.M. Stéphan, M. Poulain, Proc. SPIE **3611** p.199 (1999).(b) F. Lissillour, P. Féron, N. Dubreuil, P. Dupriez, M. Poulain, G.M. Stéphan, Elec. Lett. **36-16**p.1382 (2000).
[7] L. Landau, L. Lifchitz, *Théorie du champ*, MIR,1989.
[8] F. Treussart, *Thèse*, Université Paris 6, 1997.
[9] J. Stratton, *Electromagnétisme*, Paris, Masson, 1960.
[10] H.M. Nussenzveig, *Diffraction effects in semi-classical scattering*, Cambridge University Press, 1992.
[11] H.C. van de Hulst, *Light scattering by small particles*, New York, Wiley, 1981.
[12] C.C. Lam, P.T. Leung, K. Young, J.O.S.A.**B 9** p. 1585 (1992).
[13] (a) V.B. Braginsky, M.L. Gorodetsky, V.S. Ilchenko, Phys. Lett. A **137** p. 393 (1989). (b) M.L. Gorodetsky, V.S. Ilchenko, Opt. Comm. **113** p.133 (1994).
[14] J.C. Knight, G. Cheung, F. Jacques, T.A. Birks, Opt. Lett. **22** p.1129 (1997).
[15] (a)N. Dubreuil, J.C. Knight, D. Leventhal, V. Sandoghdar, J.Hare, V. Lefévre-Seguin, Opt. Lett. **20** p. 813 (1995). (b)V.S. Ilchenko, X.S. Yao, L. Maleki, Opt. Lett. **24** p.723 (1999).(c) B.E. Little, J.P. Laine, D.R. Lim, H.A. Haus, L.C. Kimmerling, S.T. Chu, Opt. Lett. **25** p.73 (2000).
[16] M.J.F. Digonnet, *Rare earth doped fiber lasers and amplifiers*, Stanford University, USA, 1993.
[17] M. Cai, O. Painter, K.J. Vahala, P.C. Sercel, Opt. Lett. **25** p. 1430 (2000).
[18] F. Lissillour, D. Messager, G.M. Stéphan, P. Féron, Opt. Lett. **26** p.1051 (2001).
[19] G.M. Stéphan, Phys. Rev. A **58** p.2458 (1998).
[20] F. Lissillour, R. Gabet, P. Féron, P. Besnard, G. Stéphan, Europhys. Lett. **55**(4) p.499 (2001).
[21] Z.P. Cai, A. Chardon,H.Y. Xu, P. Féron, G. Stéphan, Opt. Comm. **203** p.301 (2002). G.M. Stéphan, H.Y. Xu, Z.P. Cai, P. Féron, M. Mortier, Proc. of SPIE **4629** p. 181 (2002).

(Manuscrit reçu le 5 mars 2003)